CrossMark

Local inertial oscillations in the surface ocean generated by time-varying winds

Shengli Chen [1,2,3] · Jeff A. Polton [2] · Jianyu Hu [1] · Jiuxing Xing [3]

Abstract A new relationship is presented to give a review study on the evolution of inertial oscillations in the surface ocean locally generated by time-varying wind stress. The inertial oscillation is expressed as the superposition of a previous oscillation and a newly generated oscillation, which depends upon the time-varying wind stress. This relationship is employed to investigate some idealized wind change events. For a wind series varying temporally with different rates, the induced inertial oscillation is dominated by the wind with the greatest variation. The resonant wind, which rotates anti-cyclonically at the local inertial frequency with time, produces maximal amplitude of inertial oscillations, which grows monotonically. For the wind rotating at non-inertial frequencies, the responses vary periodically, with wind injecting inertial energy when it is in phase with the currents, but removing inertial energy when it is out of phase. The wind rotating anti-cyclonically with time is much more favorable to generate inertial oscillations than the cyclonic rotating wind. The wind with a frequency closer to the inertial frequency generates stronger inertial oscillations. For a diurnal wind, the induced inertial oscillation is dependent on latitude and is most significant at 30 °. This relationship is also applied to examine idealized moving cyclones. The inertial oscillation is much stronger on the right-hand side of the cyclone path than on the left-hand side (in the northern hemisphere). This is due to the wind being anti-cyclonic with time on the right-hand side, but cyclonic on the other side. The inertial oscillation varies with the cyclone translation speed. The optimal translation speed generating the greatest inertial oscillations is 2 m/s at the latitude of 10 ° and gradually increases to 6 m/s at the latitude of 30 °.

Keywords Inertial oscillations · Wind · Cyclone

Responsible Editor: Dieter Wolf-Gladrow

✉ Jianyu Hu
hujy@xmu.edu.cn

[1] State Key Laboratory of Marine Environmental Science, College of Ocean & Earth Sciences, Xiamen University, Xiamen 361102, China

[2] National Oceanography Centre, Liverpool L3 5DA, UK

[3] Division of Ocean Science and Technology, Graduate School at Shenzhen, Tsinghua University, Shenzhen 518055, China

1 Introduction

Historic observations report energetic inertial oscillations being generated in the ocean during the passage of storms (e.g., Saelen 1963; Day and Webster 1965; Hunkins 1967; Webster 1968). A linear wind-driven model with a decay term can reproduce the amplitude, phase and intermittency of observed inertial oscillations in the mixed layer very well, suggesting that the inertial response is predominantly locally generated by sea surface winds (Pollard and Millard 1970).

The resonant wind, which rotates anti-cyclonically with the local inertial frequency at a fixed location, can generate very strong inertial oscillations (Crawford and Large 1996; Skyllingstad et al. 2000). In practice, however, the wind is usually non-resonant. A sudden wind change can also be effective at generating inertial oscillations (Pollard 1970), which has been frequently observed during the passage of atmospheric fronts and tropical cyclones (e.g., D'Asaro 1985; Shay and Elsberry 1987; Zheng et al. 2006; Sun et al. 2011). There are many other types of wind change events that result in inertial oscillations that have not been reported and discussed. For example, some wind change events, though dramatic, may only generate weak inertial oscillations. Thus, a

systematic review on different types of wind change events is necessary and helpful and will be the main topic of this paper.

In our study, a direct relationship between inertial oscillations and changes of the wind stress is derived from a linear model (Section 2). The relationship is then employed to discuss the effect of several idealized types of wind events (Section 3), namely, the wind varying at different rates, the winds rotating anti-cyclonically or cyclonically at different frequencies with time, and the diurnal wind. We also apply this relationship to interpret effects of an idealized cyclone and the dependence on parameters of the cyclone (Section 4). The summary is presented in Section 5.

2 A simple linear model of inertial oscillations

An inertial current in the mixed layer can be well simulated by a linear slab model (Pollard and Millard 1970):

$$\frac{\partial \mathbf{u}}{\partial t} + if\mathbf{u} = \frac{1}{\rho}\frac{\boldsymbol{\tau}}{H} - r\mathbf{u} \tag{1}$$

where the current ($\mathbf{u}$, written in a complex form) and the wind stress ($\boldsymbol{\tau}$) are assumed uniform in the mixed layer (with a thickness of H). The inertial frequency is denoted by f, and the seawater density by ρ, which are both taken as constants. The damping coefficient r that is an inverse of the e-folding decay time parameterizes damping processes. Naturally, this linear model does not fully represent inertial processes. For example, without a pressure gradient term, it is a single-point model in which there is no interaction between points at nearby positions, and only local processes are considered. Furthermore, the slab nature assumes an instantaneous vertical propagation of information throughout the slab. Nevertheless, it can generally well reproduce amplitude and phase of inertial oscillations in the mixed layer (Pollard and Millard 1970; Kundu 1976; Pollard 1980). It has also been widely used to calculate the inertial energy flux from the wind (D'Asaro 1985; Alford 2001; Watanabe and Hibiya 2002; Alford 2003; Mickett et al. 2010).

The Eq. (1) can be written as:

$$\frac{\partial \mathbf{u}}{\partial t} + \omega\mathbf{u} = \frac{1}{\rho}\frac{\boldsymbol{\tau}}{H} \tag{2}$$

where

$$\omega = if + r \tag{3}$$

The solution of Eq. (2) is

$$\mathbf{u}(t) = \mathbf{C}e^{-\omega t} + e^{-\omega t}\int e^{\omega t}\frac{\boldsymbol{\tau}(t)}{\rho H}dt \tag{4}$$

where $\mathbf{C}$ is the value determined by the initial condition. Integration by parts gives

$$\mathbf{u}(t) = \mathbf{C}e^{-\omega t} + \frac{\boldsymbol{\tau}(t)}{\rho H\omega} - \frac{e^{-\omega t}}{\rho H\omega}\int e^{\omega t}\frac{d\boldsymbol{\tau}(t)}{dt}dt \tag{5}$$

On the right-hand side of Eq. (5), the second term is the instantaneous Ekman 'steady' transport. Since ω is the sum of if and r, the Ekman transport is not exactly at 90° to the wind direction, as the friction term has a veering effect. The other two terms are both related to inertial oscillations. The first term represents the initial condition of the existing inertial oscillation and can be associated with a pre-existing inertial oscillation. The third term is associated with the inertial oscillation that is newly generated by the evolving wind stress. Note that the third term vanishes under the condition that no change in wind stress occurs, i.e., for steady wind stress, whereby pre-existing inertial oscillations are preserved.

For a sufficiently short time interval Δt, the wind stress can be approximated as piecewise linear, with a constant rate of change,

$$\mathbf{A_n} = \left(\boldsymbol{\tau}(t_{n+1}) - \boldsymbol{\tau}(t_n)\right)\big/\Delta t \tag{6}$$

where $\mathbf{A_n}$ is a complex value. Substitution of $\mathbf{A_n}$ into Eq. (5) yields the velocity expression during the period ($t_n \leq t \leq t_{n+1}$)

$$\mathbf{u}(t) = \mathbf{C_n}e^{-\omega t} + \frac{\boldsymbol{\tau}(t)}{\rho H\omega} - \frac{\mathbf{A_n}}{\rho H\omega^2} + \frac{\mathbf{A_n}}{\rho H\omega^2}e^{-\omega(t-t_n)} \tag{7}$$

where $\mathbf{C_n}$ is the corresponding initial value. For convenience, the inertial terms are collected and denoted by $\mathbf{I_n}$,

$$\mathbf{u}(t) = \frac{\boldsymbol{\tau}(t)}{\rho H\omega} - \frac{\mathbf{A_n}}{\rho H\omega^2} + \mathbf{I_n}e^{-\omega(t-t_n)} \tag{8a}$$

where

$$\mathbf{I_n} = \mathbf{C_n}e^{-\omega t_n} + \frac{\mathbf{A_n}}{\rho H\omega^2} \tag{8b}$$

Similarly, the velocity during the previous interval, $t_{n-1} \leq t \leq t_n$, is

$$\mathbf{u}(t) = \frac{\boldsymbol{\tau}(t)}{\rho H\omega} - \frac{\mathbf{A_{n-1}}}{\rho H\omega^2} + \mathbf{I_{n-1}}e^{-\omega(t-t_{n-1})} \tag{9a}$$

where

$$\mathbf{I_{n-1}} = \mathbf{C_{n-1}}e^{-\omega t_{n-1}} + \frac{\mathbf{A_{n-1}}}{\rho H\omega^2} \tag{9b}$$

Assuming the flow is piecewise continuous at the time $t = t_n$, the velocity expressed in Eq. (8a) equals to that in Eq. (9a) when $t = t_n$. Therefore,

$$\mathbf{I_n} = \mathbf{I_{n-1}} e^{-\omega \Delta t} + \frac{\mathbf{A_n} - \mathbf{A_{n-1}}}{\rho H \omega^2} \tag{10}$$

i.e.,

$$\mathbf{I_n} = \mathbf{I_{n-1}} e^{-if\Delta t} e^{-r\Delta t} + \frac{\mathbf{A_n} - \mathbf{A_{n-1}}}{\rho H \omega^2} \tag{11}$$

which reveals that the inertial oscillation is composed of two parts. The first part depends on the forcing and solution of the previous interval (which decays at a rate given by the coefficient r, whilst turning anti-cyclonically by an angle of $f\Delta t$). The second part is due to variation of the wind stress. The relative size of these two parts varies with time, and the magnitude of the total inertial response depends on their relative magnitude and phase. As long as the time series of wind stress is known, Eq. (11) can be easily employed to iteratively calculate the inertial response. This has been verified with real winds, reproducing the observed near-inertial motion well, especially during the period with relatively strong wind (Chen 2014).

3 Tests for idealized varying wind scenarios

In this section, Eq. (11) is used to investigate the variation of inertial oscillations induced by some idealized types of wind change events. For convenience, Eq. (11) is rewritten in the following form:

$$\mathbf{I_n} = \mathbf{P_n} + \mathbf{N_n} \tag{12a}$$

$$\mathbf{P_n} = \mathbf{I_{n-1}} e^{-r\Delta t} e^{-if\Delta t} \tag{12b}$$

$$\mathbf{N_n} = \left(\mathbf{A_n} - \mathbf{A_{n-1}}\right) \big/ \rho H \omega^2 \tag{12c}$$

where $\mathbf{P_n}$ represents the pre-existing inertial oscillation, and $\mathbf{N_n}$ the newly wind-driven inertial oscillation. The damping coefficient (r) is set as a typical value of $(4 \text{ day})^{-1}$ (D'Asaro 1985). The mixed layer depth is assumed to be 50 m. The inertial frequency (f) is 10^{-4} rad/s (corresponding to the latitude of 43.4 ° N). The time step is 1 h. These values remain unchanged in all cases for this section.

3.1 Wind with unchanged direction

A simple case to consider is when wind only changes in magnitude. As seen in Fig. 1a, the wind examined is taken as eastward. For the first hour, the speed increases from 0 to 5 m/s (corresponding to a wind stress of 0.04 N/m², using the wind drag coefficient of Large and Pond (1981)), and
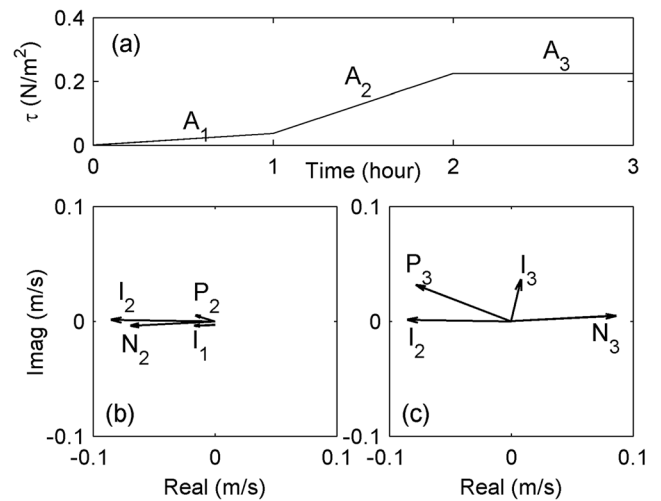

Fig. 1 Variation of wind stress with time (**a**) and induced inertial oscillations plotted in the complex plane for the first 2 h (**b**) and the third hour (**c**). The meaning of each abbreviation is as in Eq. (12a)

increases from 5 to 12 m/s (corresponding to 0.22 N/m²) for the second hour, and is then maintained at 12 m/s. The associated wind stress has the greatest rate of change during the second hour. Figure 1b, c shows the components of the resulting inertial oscillation.

For the first hour, an oscillation $\mathbf{I_1}$ is generated. At $t = 1$ h, $\mathbf{I_1}$ has rotated clockwise by an angle of $f\Delta t$ and decayed by a factor of $e^{-r\Delta t}$ to become $\mathbf{P_2}$ (Eq. 12b and Fig. 1b). At the same time, a change of the wind stress induced a new oscillation $\mathbf{N_2}$ of which the magnitude is proportional to variation of the wind stress (Eq. 12c). Since the rate of wind change during the second hour is much greater than that of the first hour (i.e., $|\mathbf{A_2}| > |\mathbf{A_1}|$), the new oscillation $\mathbf{N_2}$ is mainly determined by $\mathbf{A_2}$. The oscillation at $t = 1$ h is the superposition of $\mathbf{P_2}$ and $\mathbf{N_2}$ (i.e., $\mathbf{I_2}$). At $t = 2$ h, $\mathbf{I_2}$ has rotated clockwise and decayed to be $\mathbf{P_3}$ (Fig. 1c). The newly generated $\mathbf{N_3}$ is still quite strong, due to a greater rate of wind change $\mathbf{A_2}$. The superposition of $\mathbf{P_3}$ and $\mathbf{N_3}$ is $\mathbf{I_3}$. If the wind remains unchanged after $t = 3$ h, the new oscillation component, $\mathbf{N_4}$, will be zero. The remaining oscillation $\mathbf{I_3}$ will rotate freely and decay gradually. During this whole period, the resulting inertial oscillation is most strongly influenced by the period of steepest wind trend during the second hour. Therefore, for a general period with varying wind, the inertial oscillation generated is likely to be dominated by the period when the wind was most rapidly changing.

3.2 Winds rotating anti-cyclonically

The resonant wind, i.e., rotating anti-cyclonically and at the local inertial frequency, has been reported to produce the maximum inertial energy (Crawford and Large 1996; Skyllingstad et al. 2000). Here, we investigate how the inertial energy is built up by the resonant wind.

Fig. 2 (a) Rotation of wind stress with time, starting eastward. The inertial oscillations plotted in the complex plane for the first 2 h (**b**), the third hour (**c**) and the fourth hour (**d**). (**e**, **f**) Time-varying inertial oscillations. The meaning of each abbreviation is as in Eq. (12a)
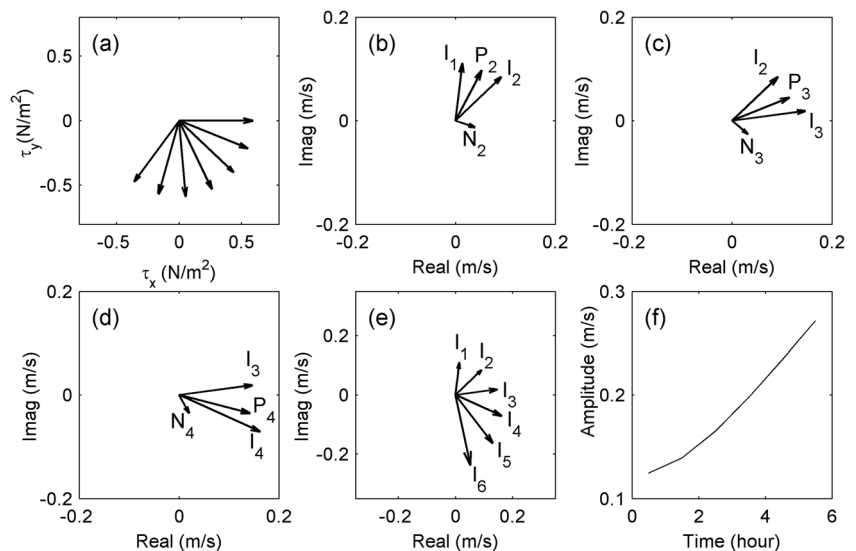

Figure 2a shows the time series of wind stress at hourly intervals. It rotates anti-cyclonically at the inertial frequency, with a constant wind speed of 18 m/s (i.e., 0.66 N/m², this value is used in all cases of rotating wind in Sections 3.2 and 3.3). During the first hour, an inertial oscillation $\mathbf{I_1}$ is produced. At $t=1$ h (Fig. 2b), $\mathbf{I_1}$ has rotated by an angle of $-f\Delta t$ to become $\mathbf{P_2}$, which combines with the newly generated oscillation $\mathbf{N_2}$ to give $\mathbf{I_2}$. Since the angle between $\mathbf{P_2}$ and $\mathbf{N_2}$ is acute, their combination $\mathbf{I_2}$ has a larger magnitude than either $\mathbf{P_2}$ or $\mathbf{N_2}$. The same situation occurs in the following time steps (Fig. 2c, d). In this way, the inertial oscillation increases monotonically with time (Fig. 2e, f).

In practice, the wind will not usually rotate at the inertial frequency. Figure 3a illustrates cases where winds of constant amplitude rotate with other frequencies. Of all cases, only the resonant wind maintains a persistently growing inertial oscillation. The response varies at the period of $2\pi/|\alpha+f|$ (cf. Section 3.4 for a detailed discussion), where α and f are the wind frequency and the inertial frequency, respectively. The oscillation of the response arises as the wind adds, and then removes, energy from the mixed layer as the wind and mixed layer motion move in and out of phase with each other. The responses of higher frequency winds ($|\alpha|>|f|$) are much greater than those of lower frequency winds ($|\alpha|<|f|$) due to greater rates of wind change (as discussed in Section 3.1). Initially, the growth rate of the response to high frequency winds even exceeds the growth rate of the resonant wind. The case of $\alpha=-1.25f$ has stronger response than that of $\alpha=-1.5f$, and the oscillation for $\alpha=-0.75f$ is stronger than that for $\alpha=-0.5f$. This indicates that the winds with frequencies closer to the inertial frequency can generate more energetic inertial oscillations, consistent with intuition.

3.3 Winds rotating cyclonically

For a wind that rotates cyclonically at the inertial frequency, the evolution of the induced inertial oscillation is shown in Fig. 4. At the first hour, an oscillation $\mathbf{I_1}$ is generated (Fig. 4b). When $t=1$ h, $\mathbf{I_1}$ has rotated clockwise by an angle of $f\Delta t$ to become $\mathbf{P_2}$, and a new oscillation $\mathbf{N_2}$ is produced. Since the angle between $\mathbf{P_2}$ and $\mathbf{N_2}$ is greater than 90 ° and they have comparable magnitudes, their superposition is smaller than the previous oscillation, i.e., $|\mathbf{I_2}|<|\mathbf{I_1}|$. It is the same case at $t=2$ h (Fig. 4c). In this way, the inertial energy is gradually removed by the wind. Overall, the amplitude varies at a period of π/f (Fig. 4d) whilst its phase change does not exhibit a gradual rotation like that induced by resonant wind. The inertial oscillation in this case is much weaker than that generated by the resonant wind.

Also examined are the cyclonic winds at other frequencies (Fig. 3b). All the responses vary periodically ($T=2\pi/|\alpha+f|$) and decay gradually. The wind with higher frequency can produce stronger inertial oscillations. However, compared with the cases of anti-cyclonic winds (Fig. 3a), the responses are much smaller. Evidently, therefore, the rotation direction of the wind plays a key role during the transfer of wind energy into inertial oscillations.

3.4 Mathematical interpretation of the response of rotating winds

The inertial oscillation associated with rotating wind can also be explored mathematically. A wind rotating with a constant amplitude (B) and at a constant frequency (α) takes a form as follows:

$$\boldsymbol{\tau}(t) = Be^{i\alpha t} \tag{13}$$

Fig. 3 Inertial oscillations generated by anti-cyclonically rotating winds (**a**) and by cyclonically rotating winds (**b**). α is the wind frequency and f is the inertial frequency
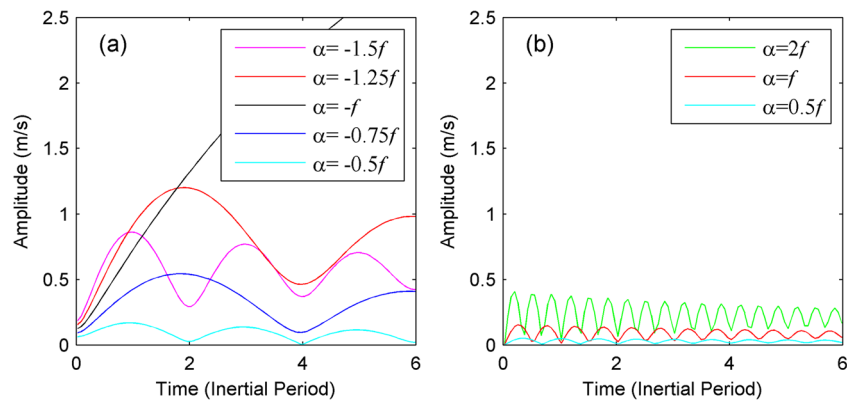
Substitution in Eq. (5) gives

$$\mathbf{u}(t) = \mathbf{C}e^{-\omega t} + \frac{Be^{i\alpha t}}{\rho H \omega} + \frac{Be^{-\omega t}}{\rho H \omega} \frac{i\alpha}{\omega + i\alpha} \left(1 - e^{(\omega + i\alpha)t} \right) \quad (14)$$

Assume the current moves from rest, i.e., when $t=0$, $\mathbf{u}=0$, which is applied to Eq. (14), yielding

$$\mathbf{u}(t) = -\left[\frac{Be^{-\omega t}}{\rho H \omega} \right]$$
$$+ \left[\left(\frac{Be^{-\omega t}}{\rho H \omega} \right) \left(\frac{i\alpha}{\omega + i\alpha} \right) \left(1 - e^{(\omega + i\alpha)t} \right) \right]$$
$$+ \left[\frac{Be^{i\alpha t}}{\rho H \omega} \right] \quad (15)$$

The first two terms (with square brackets) in Eq. (15) are associated with inertial oscillations. The magnitude of the first term depends upon the wind magnitude. The second term is the product of three parts (with round brackets). The first part is the same as the first term. The other two parts (named $\mathbf{C}_\alpha$ and $\mathbf{C_t}$) take the forms as follows:

$$\mathbf{C}_\alpha = \frac{i\alpha}{\omega + i\alpha} = \frac{1}{1 + f \big/ \alpha - ir \big/ \alpha} \quad (16)$$

$$\mathbf{C_t} = 1 - e^{(\omega + i\alpha)t} = 1 - e^{rt} e^{i(\alpha + f)t} \quad (17)$$

It shows $\mathbf{C_t}$ varies at a period of $2\pi/|\alpha + f|$, which explains the periodic tendency mentioned in Sections 3.2 and 3.3. Assuming f is fixed (10^{-4} rad/s), the magnitude of $\mathbf{C}_\alpha$ is shown as a function of f/α in Fig. 5. $\mathbf{C}_\alpha$ is symmetric along $f/\alpha = -1$, where the major peak occurs and corresponds to the resonant wind case. The closer f/α tends to negative unity, the greater the magnitude becomes. This explains why the wind with a frequency closer to the inertial frequency can generate stronger inertial oscillations. Also, it is evident that anti-cyclonic winds ($f/\alpha < 0$) have much larger values of $\mathbf{C}_\alpha$ than cyclonic winds ($f/\alpha > 0$) and, therefore, produce much more energetic inertial oscillation.

3.5 Diurnal winds

In coastal regions, the across-shore temperature gradient changes its sign over the course of the day and commonly drives a diurnal wind—the sea breeze (Simpson 1994). Theoretically, the diurnal wind could generate significant inertial oscillations (Craig 1989; Ingel 2015), which have been reported in both ocean (e.g., Simpson et al. 2002; Zhang et al. 2009; Hyder et al. 2011; Dippe et al. 2015) and atmosphere (Stockwell et al. 2004; Shibuya et al. 2014). Here, the inertial oscillation in the surface ocean produced by diurnal winds is investigated.

The wind is set to vary as a sine function with a period of 24 h and an amplitude of 10 m/s. The induced inertial oscillation is evidently dependent on latitude (Fig. 6). When the latitude is 30 °, such that the inertial frequency (f) equals the
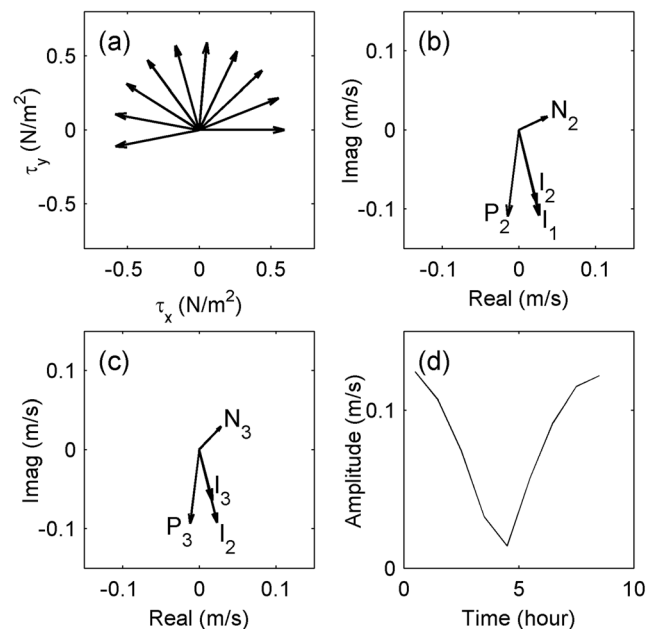

Fig. 4 (**a**) Rotation of wind stress with time, starting eastward. The inertial oscillations plotted in the complex plane for the first 2 h (**b**) and the third hour (**c**). (**d**) The variation of the inertial oscillation with time. The meaning of each abbreviation is denoted as in Eq. (12a)
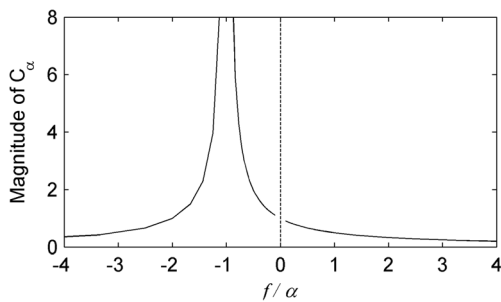
Fig. 5 The magnitude of $\mathbf{C}_\alpha$ as a function of f/α. The inertial frequency f is a constant of 10^{-4} rad/s. *Positive values* of f/α correspond to cyclonic winds, and *negative values* are for anti-cyclonic winds

diurnal frequency, the inertial oscillation grows unboundedly. At a lower latitude of 20°, the response is comparable with the case of 30° in the first 2 days, but becomes smaller later on. The responses at higher latitudes (40 and 50°) are small, even much weaker than the case of 20°. This is because the wind frequency is greater than the inertial frequency at lower latitude, however, smaller than the inertial frequency at higher latitude. In reality, inertial oscillations in the shelf region are usually damped by friction. For the seas near the latitude of 30° where this suppressing effect is weak, the inertial oscillation generated by diurnal wind could be significant.

4 Application to idealized cyclones

It is well known that the passage of a cyclone can generate intense inertial oscillations (e.g., Price 1981; Zheng et al. 2006; Sun et al. 2011). In this section, we first investigate the structure of cyclone-induced inertial oscillations. Then, the dependence on cyclone parameters (translation speed, occurring latitude, maximum wind radius) is discussed.

Assume the cyclone moves eastward along the middle line of a rectangle region (1200 km×600 km). The wind field used is idealized (Chang and Anthes 1978). The wind stress varies
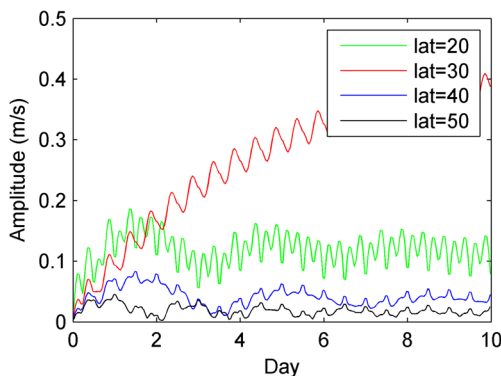

Fig. 6 The amplitude of inertial oscillations generated by diurnal winds at different latitudes

linearly with distance and does not contain asymmetry. The radial ($\tau_{rad}(r)$) and tangential ($\tau_{tan}(r)$) stresses are as follows:

$$\tau_{rad}(r) = \begin{cases} \dfrac{r}{R_1}\tau_{rad}^0 & (r \leq R_1) \\ \dfrac{R_2-r}{R_2-R_1}\tau_{rad}^0 & (R_1 \leq r \leq R_2) \\ 0 & (r \geq R_2) \end{cases} \tag{18a}$$

$$\tau_{tan}(r) = \begin{cases} \dfrac{r}{R_1}\tau_{tan}^0 & (r \leq R_1) \\ \dfrac{R_2-r}{R_2-R_1}\tau_{tan}^0 & (R_1 \leq r \leq R_2) \\ 0 & (r \geq R_2) \end{cases} \tag{18b}$$

where r is the distance away from the cyclone centre, R_1 the radius of maximum wind and R_2 the radius to the cyclone edge. τ_{rad}^0 and τ_{tan}^0 are the maximum radial and tangential wind stresses, respectively. The time series of wind stress for each position is used to compute inertial oscillations by Eq. (11), where the damping coefficient (r) and the mixed layer depth (H) are set as (4 day)$^{-1}$ and 50 m, respectively.

4.1 An initial case

In this case, the cyclone moves at a speed of 5 m/s. Other wind parameters are set as follows: R_1=50 km, R_2=300 km, τ_{rad}^0= 1.0 N/m^2, τ_{tan}^0=3.0 N/m^2. The inertial frequency is uniform (5×10^{-5} rad/s, corresponding to a latitude of 20° N).

As seen in Fig. 7, the induced inertial oscillation is intense near the cyclone centre. It is much greater on the right-hand side of cyclone's path ($y<0$) than on the left-hand side ($y>0$). The highest value occurs near the radius of maximum wind. A similar right-bias temperature cooling after a cyclone passage is a well-known phenomenon (e.g., Chang and Anthes 1978). Price (1981) attributes it to the asymmetry of near-inertial motions, which can induce enhanced mixing.

The asymmetry in the inertial response is due to different rotation directions of the wind, as has already been shown by Price (1981) for the case of a hurricane. Here, the winds at different positions are investigated in detail (Fig. 8). The wind on the right-hand side ($y<0$, Fig. 8c, d) along the cyclone's path rotates anti-cyclonically with time, whereas the wind on the left-hand side ($y>0$, Fig. 8a, b) is cyclonic. It has been shown in Section 3 how the anti-cyclonic wind produces much larger inertial oscillation than the cyclonic wind. Note that the wind rotates at a varying frequency, which increases with proximity to the cyclone centre. This suggests the wind induced by a cyclone will rarely exactly match the resonant frequency of inertial oscillations, though it could possibly be near resonant for a short period. The wind magnitude is also time dependent. For the positions outside the radius of maximum wind (Fig. 8a, d), the wind reaches its maximum amplitude when the cyclone centre is closest. For the positions inside the
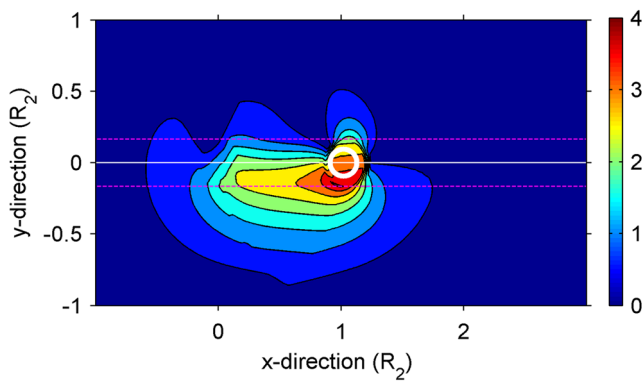
Fig. 7 The horizontal distribution of the inertial oscillation amplitude (m/s) when the cyclone centre (the *white circle*) is located at x=R_2. The *pink lines* are the radius of maximum wind (y=±50 km). The coordinates are scaled by the cyclone radius (300 km)

radius of maximum wind (Fig. 8b, c), local wind maxima are attained twice.

4.2 Varying cyclone parameters

Previous research suggests that sea surface cooling is enhanced for slow-moving cyclones (e.g., Price 1981; Mei and Pasquero 2013). Firstly, we investigate the cyclones with varying translation speeds, ranging from 1 to 12 m/s (12 cases in total). All other parameters are the same as the case in Section 4.1.

When the cyclone moves as slowly as 2 m/s, the induced inertial oscillation is very weak (Fig. 9a). With an increasing translation speed, the amplitude of the inertial oscillation increases (Fig. 9b). This is because a cyclone moving faster generates winds with a higher local rotation frequency. However, when a cyclone moves faster, it also passes the region more quickly, with less time to influence it, as seen in the case of 8 m/s (Fig. 9c). Thus, an optimal translation speed that produces the highest inertial energy levels should be the best match of wind intensity and influence duration. As shown in Fig. 10, for these parameters, the optimal translation speed is found to be around 4 m/s.

The optimal translation speed is also dependent on the latitude (Fig. 11a). At 10 °N, the optimal speed is around 2 m/s. With increasing latitude, this speed increases gradually and

reaches 6 m/s at 30 ° N. The speed increases with latitude as a function of the inertial frequency, since at high latitudes with greater inertial frequencies, a faster translating cyclone is required to generate winds that rotate at a faster rate. However, when the radius of maximum wind, R_1, is changed, the optimal translation speed remains constant at 4 m/s, though the amplitude of the inertial response does increase with the radius of maximum wind, R_1 (Fig. 11b).

5 Summary and discussion

A new relationship between the amplitude of inertial oscillations and the wind stress is derived from a set of linear momentum equations. The relationship shows that inertial oscillations are determined by the superposition of two parts (Eq. (11)): one is associated with previous inertial motion; the other is newly generated and depends upon the time-varying wind stress.

Using this relationship, the variation of inertial oscillations can be easily calculated from a time series of wind stress. This relationship is employed to investigate the inertial response to some idealized wind change events. When the wind direction does not change, but the wind magnitude varies at different rates, the resulting inertial oscillation is dominated by the wind from the period with greatest variation.

When the wind is resonant (rotating anti-cyclonically at the inertial frequency with time), the phase difference between the previous oscillation and the new oscillation is always acute. Thus, their superposition has greater magnitude than either component. Consequently, a strong inertial oscillation grows monotonically. When the anti-cyclonic wind rotates at other frequencies, a weaker inertial oscillation is generated. The amplitude of inertial oscillation varies at a period of $2\pi/|\alpha+f|$ (where α and f are the wind frequency and the inertial frequency, respectively), which increases for the first half period, but declines at the second half period. The wind with a frequency closer to inertial frequency can induce stronger inertial oscillations. When the wind rotates cyclonically with time, the inertial oscillation also varies at the period of $2\pi/|\alpha+f|$, but is much smaller in amplitude compared with that generated by anti-cyclonic winds.

Fig. 8 The wind stress (N/m^2) rotating with time at different *y* positions along the section of *x*= 300 km. Stress vectors are plotted with an interval of 2 h (shown from *blue* to *red*)
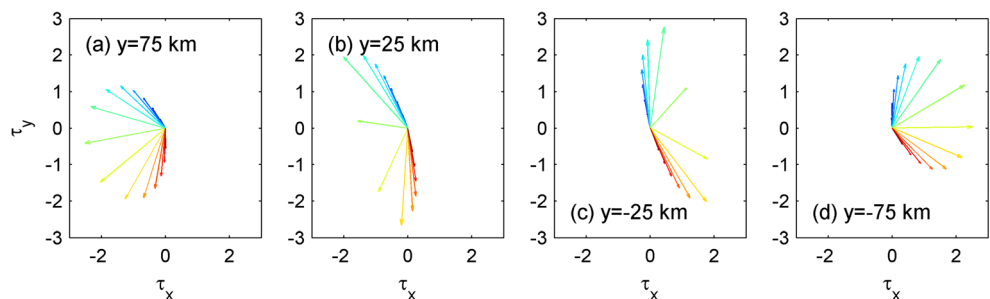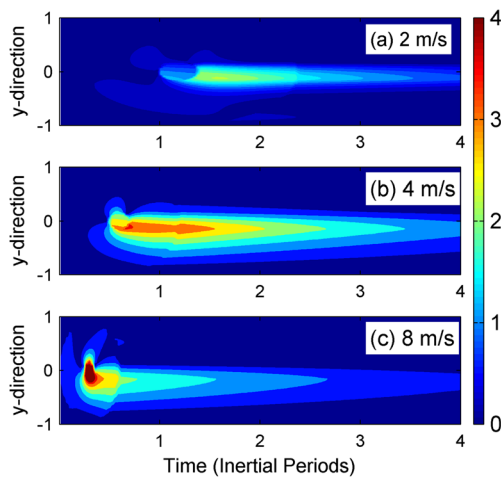
Fig. 9 Time-space (*y*) distribution of the inertial oscillation (m/s) at the section of *x*=300 km associated with different translation speeds. The time is scaled by the inertial period and the *y* space by the cyclone radius (300 km)

When the wind is diurnal (i.e., sea breeze), the inertial oscillation can also be significant and is maximal at the latitude of 30 °. However, diurnal wind mostly occurs in a coastal region where the dissipation heavily suppresses the growth of inertial oscillations. In regions where the dissipation is small, the diurnal wind will probably generate significant inertial oscillations.

The relationship between the time-varying wind stress and its inertial response is also applied to study idealized cyclones. Intense inertial oscillations are located on the right-hand side of the cyclone path (in the northern hemisphere). This is because the wind at a fixed point, on this side of the cyclone, rotates anti-cyclonically with time and can phase lock with the inertial oscillation. However, the wind on the left-hand side of the path is cyclonic and can therefore never phase lock with the inertial oscillation.

Cyclones moving at a speed ranging from 1 to 12 m/s are compared. If the translation speed is reduced, then the amplitude of inertial oscillations is also reduced, though the cyclone can force the ocean for a longer duration. Alternatively, if the
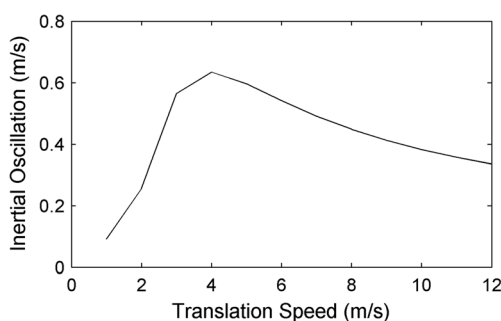

Fig. 10 The mean amplitude of inertial oscillations induced by cyclones with different translation speeds. For each cyclone case with a specific translation speed, a value is obtained by averaging the inertial oscillation at the section *x*=300 km over the first five inertial periods
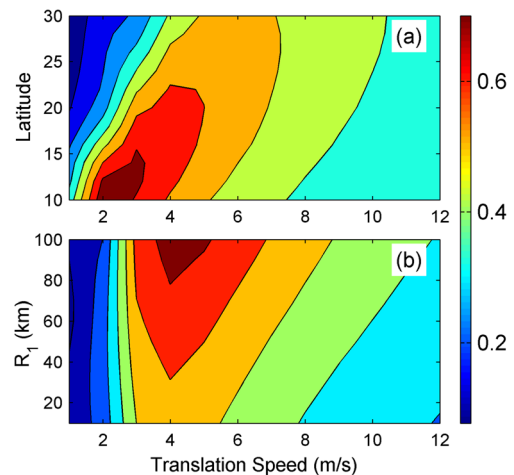

Fig. 11 (**a**) The mean amplitude of inertial currents (m/s) induced by cyclones with different translation speeds and occurring at different latitudes. For each cyclone case with a specific translation speed and at a specific latitude, a value is obtained by averaging the inertial oscillation at the section *x*=300 km over the first five inertial periods. (**b**) The mean amplitude of inertial currents (m/s) induced by cyclones with different translation speeds and different radius of maximum wind. For each cyclone case with a specific translation speed and a specific radius of maximum wind, a value is obtained by averaging the inertial oscillation at the section *x*=300 km over the first five inertial periods

translation speed is increased, then the amplitude of inertial oscillations is increased, though the cyclone forces the ocean for a shorter duration. This optimal translation speed is dependent on latitude, which is 2 m/s at 10 °, and gradually increases to 6 m/s at 30 °. This is because at higher latitude, the inertial frequency is greater, which requires a match of higher wind frequency, and thus a quicker translation speed. If the radius of maximum wind is also variable, then the optimal translation speed is not found to change. However, a cyclone with a larger radius generates greater inertial oscillations.

References

Alford MH (2001) Internal swell generation: the spatial distribution of energy flux from the wind to mixed-layer near-inertial motions. J Phys Oceanogr 31:2359–2368

Alford MH (2003) Improved global maps and 54-year history of wind-work on ocean inertial motions. Geophys Res Lett. doi:10.1029/2002GL016614

Chang SW, Anthes RA (1978) Numerical simulations of the ocean's nonlinear, baroclinic response to translating hurricanes. J Phys Oceanogr 8:468–480

Chen S (2014) Study on several features of the near-inertial motion. Dissertation, Xiamen University (In Chinese)

Craig P (1989) A model of diurnally forced vertical current structure near 30 latitude. Cont Shelf Res 9:965–980

Crawford GB, Large WG (1996) A numerical investigation of resonant inertial response of the ocean to wind forcing. J Phys Oceanogr 26: 873–891

D'Asaro EA (1985) The energy flux from the wind to near-inertial motions in the surface layer. J Phys Oceanogr 15:1043–1059

Day CG, Webster F (1965) Some current measurements in the Sargasso Sea. Deep-Sea Res 12:805–814

Dippe T, Zhai X, Greatbatch RJ, Rath W (2015) Interannual variability of wind power input to near-inertial motions in the North Atlantic. Ocean Dyn 65:859–875

Hunkins K (1967) Inertial oscillations of Fletcher's ice island (T-3). J Geophys Res 72:1165–1174

Hyder P, Simpson JH, Xing J, Gill ST (2011) Observations over an annual cycle and simulations of wind-forced oscillations near the critical latitude for diurnal-inertial resonance. Cont Shelf Res 31:1576–1591

Ingel LK (2015) One type of resonance phenomena in the atmosphere and water bodies. Fluid Dyn 50:494–500

Kundu PK (1976) An analysis of inertial oscillations observed near Oregon coast. J Phys Oceanogr 6:879–893

Large WG, Pond S (1981) Open ocean momentum flux measurements in moderate to strong winds. J Phys Oceanogr 26:3745–3765

Mei W, Pasquero C (2013) Spatial and temporal characterization of sea surface temperature response to tropical cyclones. J Phys Oceanogr 11:324–336

Mickett JB, Serra YL, Cronin MF, Alford MH (2010) Resonant forcing of mixed layer inertial motions by atmospheric easterly waves in the northeast tropical pacific. J Phys Oceanogr 40:401–416

Pollard RT (1970) On the generation by winds of inertial waves in the ocean. Deep Sea Res 17:795–812

Pollard RT (1980) Properties of near-surface inertial oscillations. J Phys Oceanogr 10:385–398

Pollard RT, Millard RC (1970) Comparison between observed and simulated wind-generated inertial oscillations. Deep Sea Res 17:153–175

Price JF (1981) Upper ocean response to a hurricane. J Phys Oceanogr 11: 153–175

Saelen OH (1963) Studies in the Norwegian Atlantic current (Part II). Geofys Publr 23:1–82

Shay LK, Elsberry RL (1987) Near-inertial ocean current response to hurricane Frederic. J Phys Oceanogr 17:1249–1269

Shibuya R, Sato K, Nakanishi M (2014) Diurnal wind cycles forcing inertial oscillations: a latitude-dependent resonance phenomenon. J Atmos Sci 71:767–781

Simpson JE (1994) Sea breeze and local wind. Cambridge University Press, Cambridge

Simpson JH, Hyder P, Rippeth TP, Lucas IM (2002) Forced oscillations near the critical latitude for diurnal-inertial resonance. J Phys Oceanogr 32:177–187

Skyllingstad ED, Smyth WD, Crawford GB (2000) Resonant wind-driven mixing in the ocean boundary layer. J Phys Oceanogr 30: 1866–1890

Stockwell RG, Large WG, Milliff RF (2004) Resonant inertial oscillations in moored buoy ocean surface winds. Tellus 56A:536–547

Sun Z, Hu J, Zheng Q, Li C (2011) Strong near-inertial oscillations in geostrophic shear in the northern South China Sea. J Oceanogr 67: 377–384

Watanabe M, Hibiya T (2002) Global estimates of the wind-induced energy flux to inertial motions in the surface mixed layer. Geophys Res Lett. doi:10.1029/2001GL014422

Webster F (1968) Observations of inertial-period motions in the deep sea. Rev Geophys 6:473–490

Zhang X, DiMarco SF, SmithIV DC, Howard MK, Jochers AE, Hetland RD (2009) Near-resonant ocean response to sea breeze. J Phys Oceanogr 39:2137–2155

Zheng Q, Lai RJ, Huang NE, Pan J, Liu WT (2006) Observation of ocean current response to 1998 Hurricane Georges in the Gulf of Mexico. Acta Oceanol Sin 25:1–15